RSC Advances

RSC Publishing

PAPER

View Article Online
View Journal

Cite this: DOI: 10.1039/c3ra42549e

One-pot preparation of unsaturated polyester nanocomposites containing functionalized graphene sheets *via* a novel solvent-exchange method†

Chengguo Liu,*[ab] Zhimin Wang,[a] Yu'an Huang,[c] Hongfeng Xie,[d] Zengshe Liu,‡[e] Ying Chen,[a] Wen Lei,[f] Lihong Hu,[ab] Yonghong Zhou*[a] and Rongshi Cheng[d]

This paper reports a convenient one-pot method integrating a novel solvent-exchange method into *in situ* melt polycondensation to fabricate unsaturated polyester nanocomposites containing functionalized graphene sheets (FGS). A novel solvent-exchange method was first developed to prepare graphene oxide/ethylene glycol (GO/EG) dispersions in a reactor equipped with a fractionating device. The prepared dispersions were applied successively to fabricate unsaturated polyester composites *via in situ* melt polycondensation in the same reactor. The dispersion behavior of GO/EG dispersions was characterized by atomic force microscopy (AFM). The structures and properties of the as-prepared FGS/polyester nanocomposites were characterized by Fourier transform infrared spectroscopy (FT-IR), X-ray diffraction (XRD), Raman spectroscopy, scanning electron microscopy (SEM), transmission electron microscopy (TEM), tensile tests, thermogravimetric analysis, and dynamic mechanical analysis. The results of AFM show that GO nanosheets are well exfoliated in EG solvent. The results of FT-IR, XRD, Raman, SEM, and TEM indicate that the FGS are also finely exfoliated in the polyester matrix and have strong interaction with the host polymer. Compared with the neat UPR matrix, the composite with an extremely low content of 0.08 wt% FGS exhibits maximum increases of 53.6% and 48.4% in tensile strength and modulus; the composite with 0.32 wt% FGS has a 10.7 °C increase in thermal decomposition temperature and a 17.9 °C increase in glass transition temperature. Therefore, building on this work to generate unsaturated polyester nanocomposites with improved properties at reduced cost is possible.

Received 23rd May 2013
Accepted 20th September 2013

DOI: 10.1039/c3ra42549e

www.rsc.org/advances

Introduction

Graphene, a one-atom-thick 2D layer of sp^2-bonded carbon, has been intensively studied since its discovery in 2004.[1–8] Its superior mechanical, thermal, and electrical properties together with its ultrahigh surface area, make graphene outstanding in fabricating various materials such as micro-electrical devices, batteries, supercapacitors, and nanocomposites.[1–8] In the preparation of graphene/polymer nanocomposites with optimized performance, the biggest problem is the exfoliation and incorporation of graphene into the polymer matrix to achieve a single-layer graphene-reinforced polymer because graphene from graphite has strong π–π stacking interactions between layers and incompatible surface characteristics with polymer matrix.

Thus far, the most promising strategy developed to address this obstacle is the employment of graphene oxide (GO) as precursor.[3–9] In contrast to pristine graphene, GO sheets possess numerous oxygen-containing groups on the surface, such as hydroxyls, epoxides, carbonyls, and carboxyls.[3–9] These functional groups significantly weaken the van der Waals interactions between the graphene layers, thus allowing the good dispersion of GO in solutions and facilitating the interaction between polymer hosts and GO *via* covalent or non-covalent bonds.[5,9–12] For example, GO and reduced GO have been successfully incorporated into water-soluble polymers such as poly(vinyl alcohol), chitosan and cellulose *via* simple solution mixing method by using water as the media.[3,8,9,13,14]

[a]*Institute of Chemical Industry of Forestry Products, CAF, National Engineering Lab. for Biomass Chemical Utilization, Key and Lab. on Forest Chemical Engineering, SFA, Key Lab. of Biomass Energy and Material, Jiangsu Province, Nanjing 210042, P. R. China. E-mail: liuchengguo@gmail.com; yhzhou777@sina.com; Fax: +86-25-85482777; Tel: +86-25-85482777*

[b]*Institute of Forest New Technology, CAF, Beijing 100091, P. R. China*

[c]*School of Material Engineering, Nanjing Institute of Technology, Nanjing 211167, P. R. China*

[d]*Key Laboratory of Mesoscopic Chemistry of Ministry of Education, College of Chemistry and Chemical Engineering, Nanjing University, Nanjing 210093, P. R. China*

[e]*Food and Industrial Oil Research, NCAUR, ARS/USDA, 1815 N. University Street, Peoria, IL 61604, USA*

[f]*College of Science, Nanjing Forestry University, Nanjing 210037, P. R. China*

† Electronic supplementary information (ESI) available. See DOI: 10.1039/c3ra42549e

‡ Mention of trade names or commercial products in this publication is solely for the purpose of providing specific information and does not imply recommendation or endorsement by the U.S. Department of Agriculture. USDA is an equal opportunity provider and employer.

Unfortunately, GO cannot be readily exfoliated in most organic solvents. Thus, further chemical modification of GO with different molecules or polymers and dissolvation of GO in the presence of dispersants or stabilizers are the two frequently-used methods to achieve molecular-level dispersions.[3,7,9]

A solvent-exchange method has recently been employed to prepare homogenous dispersions of GO or graphene in different organic solvents such as *N*,*N*-dimethylformamide (DMF),[14] dimethyl sulfoxide (DMSO),[14,15] silicone oil,[16] terpineol,[17] and ethanol.[18,19] Fine liquid dispersions of GO or graphene without the help of chemical modification, dispersants or stabilizers could be prepared through this simple method, relying on the large difference of the exchanged solvents in boiling points.[14–18] However, as one of the widely-used monomers (solvents) in the synthesis of polyesters, low-molar-mass diols such as ethylene glycol (EG) have not yet been reported in the preparation GO dispersions through this method.

On the other hand, graphene-based polymer composites are commonly prepared by solution mixing, melt compounding, and *in situ* polymerization.[8] The *in situ* polymerization approach is particularly remarkable because it enables control over both the polymer architecture and the final structure of the nanocomposites. Numerous graphene-based polymer composites have been successfully prepared through this method, including graphene/polystyrene,[20,21] graphene/poly(methyl methacrylate),[22] graphene/epoxy,[23–26] graphene/polyurethane,[27–29] graphene/nylon,[30–32] graphene/polypropylene,[33] graphene/polyimide,[34] and graphene/poly(ethylene terephthalate).[35] This approach involves a two-step procedure: dispersing GO sheets well in organic solvents or monomers, followed *via in situ* polymerization initiated by heat, light or other suitable reagents. Since graphite oxide prepared by Staudenmaier or Hummers method[36–40] is not so readily exfoliated in some organic solvents (*e.g.*, EG) as in water, the solvent-exchange method could be appropriately applied to prepare GO dispersions in organic solvents.

Based on the above consideration, a convenient one-pot method that integrates solvent-exchange method into *in situ* melt polycondensation is developed for the first time to fabricate polyester nanocomposites in this work. At the stage of melt polycondensation for polyesters, fractional distillation technique is always employed to separate the generated water from the reacting mixture and largely reduce the loss of diols. This technique can also be applied in the solvent-exchange method. Thus a novel solvent-exchange method consisting of fraction distillation is first developed to prepare GO/EG dispersions. In this one-pot method, the as-prepared GO/EG dispersions can be consecutively applied to fabricate polyester nanocomposites *via in situ* melt condensation without changing the reactor. Unsaturated polyesters resin (UPR), currently one of the most widely-used thermosetting polymers, is chosen as the host polymer mainly because it possesses inferior stiffness to other resins like epoxy, which limits its application in high-added-value areas such as aerospace, marine and blade of wind power. Considering the probable partial reduction of GO sheets during the preparation of UPR,[34,35] functionalized graphene sheets (FGS) are employed in the obtained UPR composites instead of GO sheets. Furthermore, the dispersion behavior of GO in EG solvent, as well as the structures and properties of the prepared FGS/UPR nanocomposites, are carefully studied.

Experimental section

Materials

Graphite powder (100 mesh) was obtained from Shanghai Colloidal Co. Ltd. Maleic anhydride (MA), phthalic anhydride (PA), and EG were obtained from Shanghai Lingfeng Chemical Reagent Co., Ltd. Potassium permanganate ($KMnO_4$), sulfuric acid (H_2SO_4, ≥98%), hydrogen peroxide (H_2O_2), hydrochloric acid, sodium nitrate ($NaNO_3$), ethanol, and potassium hydroxide (KOH) were obtained from Kermel Chemical Reagent Co., Ltd. Styrene (St, ≥98%) and the inhibitor hydroquinone (≥98%) were obtained from Chengdu Kelong Chemical Reagent Co., Ltd. The initiator benzoyl peroxide (≥98%) and the promoter *N*,*N*-dimethylaniline (≥98%) were obtained from Aladdin Chemistry Co., Ltd. The EG and St were dried by molecular sieves for at least one week before use. All the other reagents were used as received.

Synthesis of UPR

A reaction mixture of EG (36 g, 0.581 mol), MA (25.9 g, 0.264 mol), PA (39.1 g, 0.264 mol), and hydroquinone (0.1 g) was added into a 250 ml four-necked flask. The flask was then equipped with mechanical stirrer, thermometer, N_2 gas inlet, and fractionating tube to transform it into a fractional distillation device (see Fig. S1 in ESI†). The reactor was subsequently heated by oil bath to 70 °C and agitated at this temperature for 30 min until the MA solid completely melted. Precondensation was conducted under N_2 atmosphere at 160 °C for 1.5 h. After gradually heating to 200 °C, the polycondensation lasted for 3 to 4 h at this temperature until the acid value of the reacting mixture decreased to a set value, at which the samples had similar molar masses. Finally, the product was blended with styrene (50 g, 33% of the total weight) and hydroquinone (0.01 g) for 1 h at 90 °C to produce a light and transparent liquid resin.

Preparation of FGS/UPR nanocomposites

The graphite oxide used in this work was prepared from graphite through the modified Hummers method.[39,40] The obtained graphite oxide was dispersed in deionized water (H_2O) through ultrasonication and centrifugation to achieve homogenous GO/H_2O dispersion (with a concentration of about 7.33 mg ml^{-1}). Using this GO/H_2O dispersion as starting material, FGS/UPR nanocomposites containing different FGS contents were prepared by a convenient one-pot method that integrates a novel solvent-exchange method into *in situ* melt polycondensation, as illustrated in Fig. 1. Typically, GO/H_2O dispersion (40 g) and EG (40 g) were added into the same device as that in the synthesis of UPR. Then, the GO/H_2O/EG mixture was vigorously stirred and the temperature of the oil bath was gradually increased to 160 °C. After fractionating for 3 h at this temperature, approximately 15 wt% of water still remained in the mixture through simple weighing. To accelerate the solvent-exchange process and remove the residual water in the mixture,

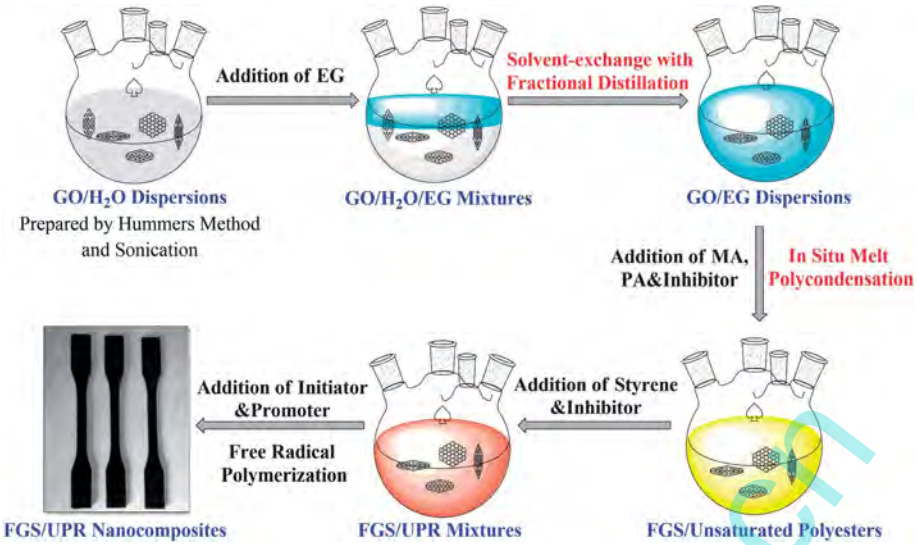

Fig. 1 Illustration of one-pot method that integrates a solvent-exchange method into *in situ* melt polycondensation to prepare FGS/UPR nanocomposites. The four-neck flask represents the reactor in the fractional distillation device.

vacuum distillation was conducted by a water pump for 15 to 30 min. After this procedure black and opaque GO/EG dispersions (about 36 g) were left in the reactor. Vacuum distillation can also modulate the product mass of GO/EG dispersion, which is important for the integration of solvent-exchange method and *in situ* polymerization. Consecutively, a mixture of MA (25.9 g, 0.264 mol), PA (39.1 g, 0.264 mol), and hydroquinone (0.1 g) was added into the reactor. The process of *in situ* melt polycondensation was the same as that described in the synthesis of UPR. Finally, black and opaque resins containing different contents of FGS were obtained.

The as-prepared neat UPR and UPRs containing different FGS contents were cured following the same procedure: blended with the initiator (1.5 wt% of the resins) for 20 min and then with the promoter (0.15 wt% of the resins) for 1 to 2 min, poured into molds, cured at room temperature for 6 h, and postcured at 60 °C for 3 h. At last the neat UPR matrix and the FGS/UPR nanocomposites were obtained. In our experiments, the contents of GO in the FGS/UPR composites were 0.04, 0.08, 0.16, and 0.32 wt%, so the composites were labeled as 0.04 % FGS/UPR, 0.08% FGS/UPR, 0.16% FGS/UPR, and 0.32% FGS/UPR. The neat UPR matrix without FGS content was marked as UPR and set as blank test.

Characterization

Atomic force microscopy (AFM) images of GO nanosheets on mica substrates from water or EG solvent were obtained using a CSPM 5000 Atomic Force Microscope (Benyuan Corporation, China) in taping mode. Fourier transform infrared (FT-IR) spectra were recorded on a Nicolet iS10 IR spectrometer (Thermo-Fisher, USA). X-ray diffraction (XRD) spectra were recorded on a D8 FOCUS X-ray diffractometer (Bruker Corporation, Germany). Raman spectra were recorded by a MultiRAM Stand Alone FT-Raman spectrometer with λ_{ex} = 1064 nm (Bruker Corporation, Germany). Scanning electron microscopy (SEM) examinations of the tensile-fractured and etched surface of the FGS/UPR composites were performed on an S-3400N Scanning Electron Microscope (Hitachi Corporation, Japan). Transmission electron microscopy (TEM) examinations of the FGS/UPR nanocomposite films were performed on a Tecnai G^{2}20 Transmission Electron Microscope (FEI Corporation, USA). Tensile tests of the neat UPR matrix and the FGS/UPR composites were performed using a SANS7 CMT-4304 Universal Tester (Xinsansi Corporation, China). Thermogravimetric analysis (TGA) was performed on an STA 409PC Thermogravimetry instrument (Netzsch Corporation, Germany) at a heating rate of 15 °C min^{-1}. Dynamic mechanical analysis (DMA) was conducted in three-point bending geometry on a Q800 solid analyzer (TA Corporation, USA).

Results and discussion

Dispersion of GO in EG solvent

The key factor for fabricating high-performance FGS/polyester nanocomposites by *in situ* melt polycondensation is the good dispersion of GO in one of the monomers (EG monomer).[35] Therefore, the dispersion state of GO/EG solutions in the intermediate state of the one-pot process should be assessed first.

By visual inspection we found that the as-prepared GO dispersions have long-term homogeneous stability (>7 days) in EG solvent, as shown in Fig. 2a. To investigate the degree of exfoliation of the GO material in both water and EG solvents, AFM imaging of their dispersions deposited onto mica substrates was carried out. Fig. 2b displays a typical tapping-mode AFM image of GO nanosheets from an aqueous dispersion after sonication treatment. The GO nanosheet has a thickness of about 1.0 nm and a length of about 2 μm, which are characteristics of a fully exfoliated GO nanosheet.[35,41] The dispersion of GO in EG solvent after sonication was also evaluated by AFM, as indicated in Fig. 2c. The GO nanosheets in EG

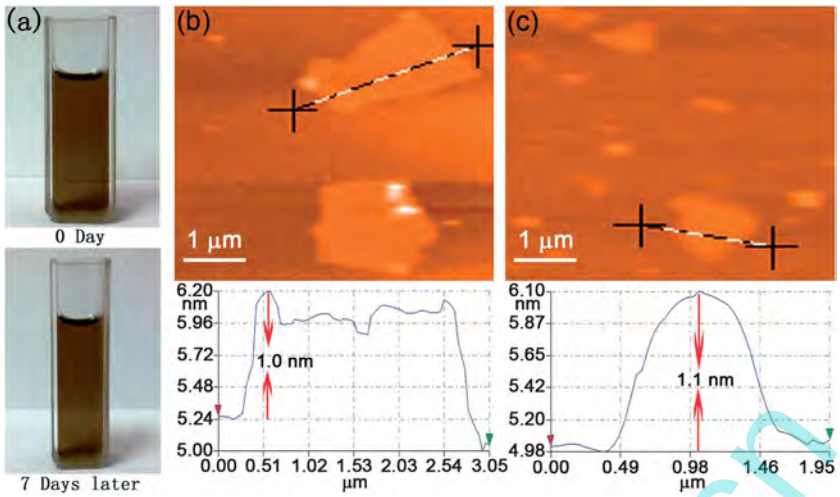

Fig. 2 (a) Photographs of the prepared GO/EG dispersion for a solution-stability experiment. AFM images and line profiles of the GO samples exfoliated in (b) water and (c) EG solvent.

solvent almost have the same thickness (about 1.1 nm) as those in water, which also indicates a good exfoliation of GO in EG solvent.[35,41] The dimension of GO sheets in EG solvent is about several hundred nanometers to several micrometers in length (see Fig. S2 in ESI†). Therefore, the GO/EG solutions were successfully prepared by this fractional distillation-assisted solvent-exchange method. By altering the amount of GO/water dispersions added, a series of GO/EG dispersions with concentrations of 1.47 to 13.0 mg ml^{-1} was prepared.

The novel solvent-exchange method in the one-pot method can be applied to other organic solvents, such as DMF, DMSO, and *N*-methyl-2-pyrrolidone. Thus, the solvent-exchange method in the one-pot method is expected to have diverse applications in fabricating GO-based nanocomposites by solution mixing or *in situ* polymerization. Compared with the solvent-exchange method involving sole vacuum distillation,[14–16] this fractionating-assisted method requires a smaller difference in boiling points between the exchanged solvents and better reduces the loss of organic solvents. By simple weighing of the solutions left in the reactor, a small amount of EG solvent (less than 10 wt% of the original addition) was observed to have been lost after 5 h fractionation in the solvent-exchange process. Moreover, with the aid of several-minutes vacuum distillation, the mass of monomers can be conveniently tuned to adjust the subsequent *in situ* polymerization of polyester nanocomposites.

Structure characterization of the FGS/UPR nanocomposites

As shown in Fig. 1 and the experiment section, the GO/EG dispersions prepared by this novel solvent-exchange method can be successively applied in fabricating UPR nanocomposites *via in situ* melt polycondensation. It is noted that the GO sheets still existed in the EG solvent after the solvent-exchange process because the characteristic thickness of the sheet is about 1.1 nm. However, GO sheets were reported to experience a simultaneous partial reduction during the *in situ* polymerization process at high temperatures.[34,35] In order to determine whether the chemical state of GO sheets changed during the high temperature polycondensation process, the GO sheets were experienced the same thermal treatment as the polycondensation process (see SI.3 section in ESI†). The resultant products for changes in the chemical state of the sheets were analyzed by FT-IR, XRD, and TGA (see Fig. S3 to S5 in ESI†). All the results indicate that GO sheets have been reduced to FGS during the high temperature polycondensation process.

The next step is to check whether FGS have been well exfoliated in the UPR matrix. FT-IR technique was first employed to study the structure of FGS/UPR nanocomposites. The FT-IR spectra of dried GO sheets, neat UPR, and their nanocomposites are depicted in Fig. 3. The dried GO sheets were obtained by drying GO/H_2O dispersions in an ordinary bake oven at 50 °C for 24 h and then in a vacuum bake oven at 50 °C for 48 h. Several characteristic peaks can be observed in the spectrum of GO: hydroxyls (3600 cm^{-1} to 2500 cm^{-1} with a maximum at

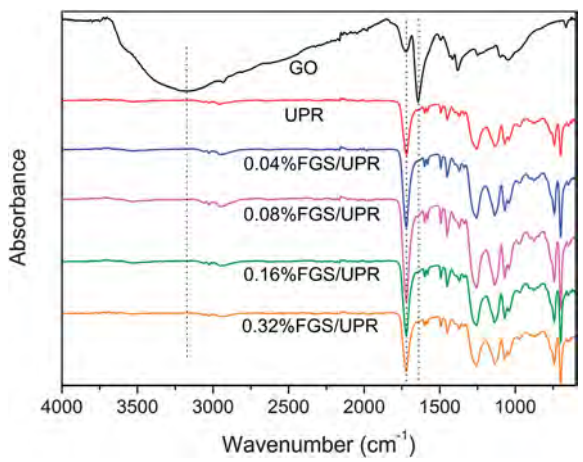

Fig. 3 FT-IR spectra of dried GO sheets, neat UPR, and FGS/UPR nanocomposites with different FGS contents.

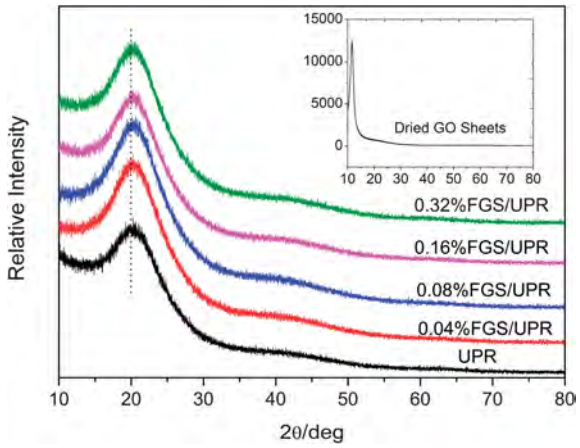

Fig. 4 XRD patterns of GO sheets, neat UPR, FGS/UPR nanocomposites with different FGS contents. The inset shows XRD pattern of dried GO sheets.

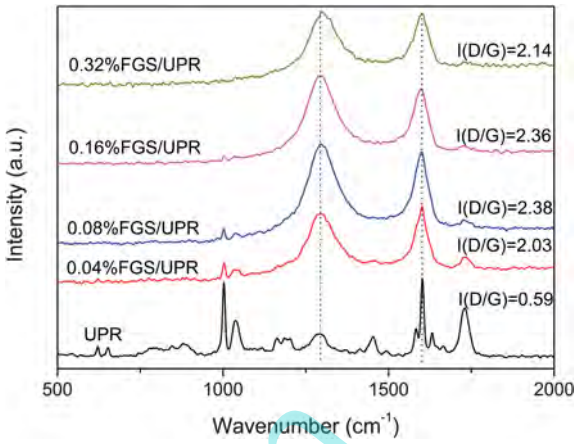

Fig. 5 Raman spectra of neat UPR and FGS/UPR nanocomposites with different FGS contents.

3182 cm^{-1}, strong and broad), C=O on carbonyl groups (1723 cm^{-1}, moderate), C=O on carboxyl groups or intercalated water (1641 cm^{-1}, strong), C–OH (1384 cm^{-1}, moderate), and C–O (1000–1300 cm^{-1}, moderate).[15,35,42–44] Some typical peaks are also present in the spectrum of neat UPR: hydroxyls (3428 cm^{-1}, very weak), C=O on ester group (1724 cm^{-1}, strong), and C–O (1000 cm^{-1} to 1300 cm^{-1}, strong). However, almost no difference in the spectra between FGS/UPR nanocomposites and neat UPR was observed, especially at the wavelengths 3182, 1724, and 1641 cm^{-1}. The disappearance of these characteristic peaks of GO sheets in the nanocomposites are probably attributed to the very low content of GO, or the reduction of GO into FGS (which is featureless in the IR spectra) during the melting polycondensation.[34,35]

XRD is another important tool employed to investigate the exfoliation of FGS in the composites. Fig. 4 shows the XRD patterns of dried GO sheets, neat UPR, and their composites. Similar to reported values,[15,43] the characteristic diffraction peak of dried GO sheets appears at approximately 11.6°, which indicates typical hydrated graphite oxide feature.[45] The neat UPR sample shows a broad peak at about 20.1°, revealing its crystallinity tendency, which results from the molecule symmetry of EG monomer. However, after the incorporation of GO into the UPR matrix, the XRD patterns of FGS/UPR composites with different FGS contents are almost the same as those of the neat UPR. The disappearance of the characteristic diffraction peak of GO sheets in these nanocomposites also indicates that FGS are fully exfoliated in the UPR matrix.[15]

Raman spectroscopy has been reported as a powerful probe for the structure of carbonaceous materials. Fig. 5 shows the Raman spectra of neat UPR and its nanocomposites with different FGS loadings. The Raman spectrum of GO sheets was not provided in this paper because the Raman spectroscopy (λ_{ex} = 1064 nm) used in this study is only sensitive to polymers, whereas the characteristic peaks of D band (1341 cm^{-1}) and G band (1596 cm^{-1}) in GO sheets have been recorded by another kind of Raman spectroscopy with a different λ_{ex} (see Fig. S6 in ESI†). The Raman spectrum of neat UPR demonstrates its characteristic peaks at 1731 cm^{-1} (C=O on ester group), 1664 cm^{-1} (C=C on polyester), 1632 cm^{-1} (C=C vinyl on styrene), 1600 cm^{-1} (C=C aromatic on polyester), 1580 cm^{-1} (C=C aromatic on styrene), 1453 cm^{-1} (C–H on polyester), 1289 cm^{-1} (CH_2 on polyester), 1184 cm^{-1} (C–O–C on polyester), and 1000 cm^{-1} (CH_2, C–C on polyester).[46,47] However, after incorporation of GO into the UPR matrix, the intensities of peaks at around 1291 cm^{-1} (D band at this λ_{ex} = 1064 nm[48] and

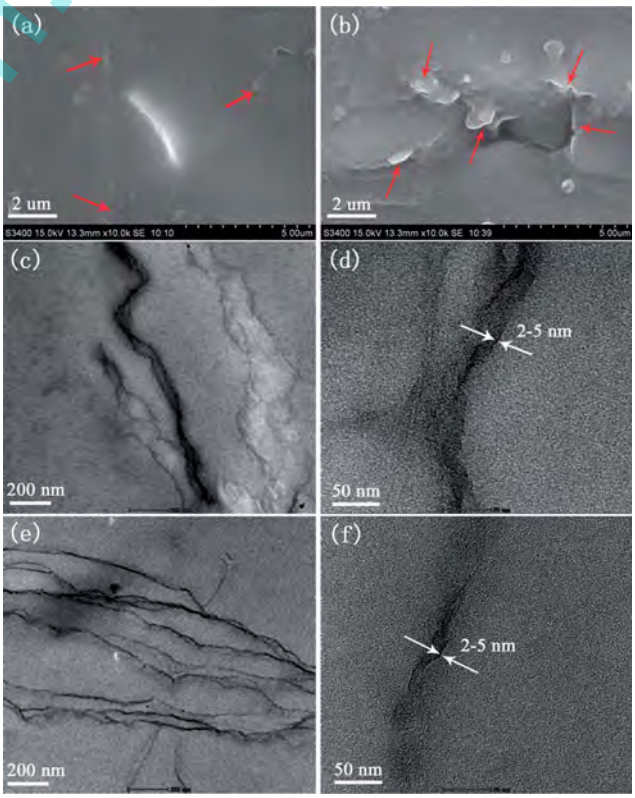

Fig. 6 SEM images of etched FGS/UPR composites with FGS contents of (a) 0.04 wt% and (b) 0.32 wt%, respectively. TEM images of FGS/UPR composite with the FGS content of 0.04 wt% at (c) low magnification and (d) large magnification as well as the composite with the FGS content of 0.32 wt% at (e) low magnification and (f) large magnification.

1600 cm^{-1} (G band) remarkably increase. The appearance of these two bands clearly demonstrates that the original GO sheets have changed into other states, *e.g.*, reduced GO, or FGS covalently-linked with polymers. Meanwhile, weak bands from UPR are seen at, *e.g.*, 1000, 1038, 1184, 1453 and 1731 cm^{-1} and their relative intensities compared with that of the two broad peaks is clearly seen to gradually decrease as the FGS content in the composites is increased. The intensity ratio of D and G bands (I(D/G)) is correlated with the disordered and ordered crystal structures of carbon and is the inverse of the average size of sp^2 domains.[49] As shown in Fig. 5, all the I(D/G) values of the composites are larger than those of the neat UPR (0.59) and the GO (1.60 in Fig. S6†). When the covalent functionalization is conducted on functional groups in the interbasal platelet of graphene, a substantial enhancement of I(D/G) was observed due to the introduction of additional defects on the graphitic lattice.[14,50–52] Therefore, It can be concluded that a strong covalent interaction exists between FGS and the UPR matrix.

SEM and TEM can directly explore the dispersion state of FGS in the UPR matrix and the interaction between them. To clearly show the dispersion of FGS, the fracture surface after the tensile test was etched in KOH–ethanol (10 wt%) solvent for 1.5 h at 40 °C. Fig. 6a and b present the etched fracture surface for the model FGS/UPR nanocomposites with FGS contents of 0.04 wt% and 0.32 wt%. The FGS (indicated by red arrows) are uniformly exfoliated in the two composites with an average length of about 0.5 to 3 μm. Moreover, the protruding FGS in the nanocomposites are not so crumpled or wrinkled and are still coated with adsorbed resins after etching, indicating strong filler–polymer interfacial interactions.[8,53] The TEM images of the ultrathin sections of the model nanocomposites containing 0.04 wt% and 0.32 wt% FGS are demonstrated in Fig. 6c–f. In these macrographs, the FGS appear as distinct dark lines homogeneously dispersed in the matrix. The FGS fillers have been successfully dispersed in the matrices with exfoliated or intercalated structures.[54] In the high-magnification images of the composites (Fig. 6d and f), the thickness of the intercalated FGS is about 2 to 5 nm (indicated by white arrows). This value is a little higher than that of the pure GO nanosheets in the AFM images, but still shows that the FGS has achieved a molecular-level dispersion in the polymer matrix.[14,34,54–56] Two major reasons could be account for the good dispersion of FGS sheets. First, the GO sheets have been well exfoliated in the EG monomers, as shown in the AFM images. Second, the functional groups on the surfaces and sides of the original GO nanosheets may have reacted with the diol or the diacid monomers during the high-temperature melt polycondensation process.[34,35] These functional groups may also form hydrogen bonds with the C=O groups on the polymer chains of UPR.[34]

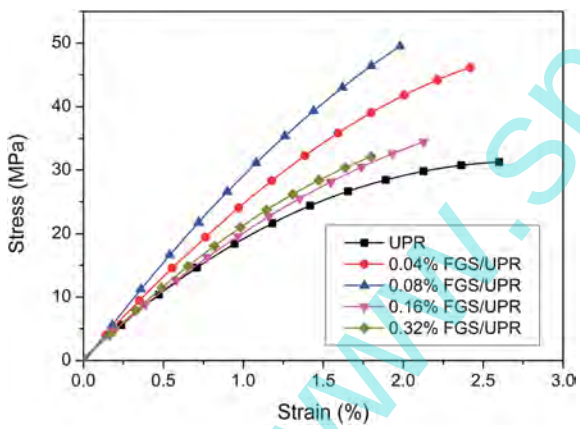

Fig. 7 Stress–strain curves of neat UPR and FGS/UPR nanocomposites with different FGS contents.

Property characterization of the FGS/UPR nanocomposites

Typical stress–strain curves of the near UPR and FGS/UPR nanocomposites are shown in Fig. 7, and the corresponding results are summarized in Table 1. For accuracy, at least five specimens were measured and the values were averaged. The tensile properties of the UPR matrix are obviously improved by the incorporation of GO sheets. Compared with the neat UPR, maximum increases of 53.6% and 48.4% in tensile strength and modulus are observed for the composite containing only 0.08 wt% FGS. Similar results about the significant mechanical effect at very-low FGS loadings have been found in GO/polybenzimidazole,[15] FGS/epoxy,[23] and FGS/poly(ethylene terephthalate)[35] nanocomposites. Such large improvement in stiffness indicates the efficient load transfer from the matrix to the FGS nanofiller, which is caused by the good exfoliation of FGS and the strong FGS–polymer interaction.[8,34,35] This improvement should also be attributed to the one-pot preparation integrating solvent-exchange method and *in situ* polymerization, in which GO nanosheets remain exfoliated all the time since in the aqueous dispersions. Notably, the

Table 1 Mechanical and thermal properties of the neat UPR and FGS/UPR composites with different FGS contents[a]

Samples	$C_{GO/EG}$ (mg ml^{-1})	Tensile strength (MPa)	Tensile modulus (GPa)	T_p (°C)	E' at 40 °C (GPa)	E' at 150 °C (MPa)	T_g (°C)
UPR	0	32.1 ± 1.5	2.46 ± 0.21	393.2	1.25	26.1	72.6
0.04% FGS/UPR	1.47	45.9 ± 1.8	3.01 ± 0.20	399.2	1.49	29.5	88.0
0.08% FGS/UPR	3.29	49.3 ± 2.3	3.65 ± 0.29	399.2	1.63	29.2	88.2
0.16% FGS/UPR	6.46	38.2 ± 1.6	2.61 ± 0.17	399.2	1.47	29.0	88.6
0.32% FGS/UPR	13.0	32.5 ± 1.1	2.81 ± 0.16	403.9	1.36	28.1	90.5

[a] $C_{GO/EG}$, T_p, E', T_g and ν_e represent GO concentration in EG solvent, thermal decomposition temperature at the maximum weight-loss rate, storage modulus, and glass transition temperature, respectively.

improvement may have little to do with the variation of crystallinity, because the addition of a large amount of styrene into the unsaturated polyester and the low FGS content result in fairly low crystallinity of all the composites (Fig. 4). In addition, the stiffness of the other three nanocomposites is still better than that of the neat UPR. However, the improvement is not as great as that for the 0.08% FGS/UPR nanocomposite, especially for the composite containing 0.32 wt% FGS. This finding probably results from the gradual FGS agglomeration at higher loading, which brought about local stress concentration and decreased the energy dissipation capability.[8,23,34,35] For example, the FGS/UPR composite with a FGS content of 0.32 wt% was prepared using a GO/EG dispersion with GO concentration up to 13.0 mg ml^{-1} (Table 1). The reason why the composite with such low FGS content (0.08 wt%) has the best stiffness is being studied in our group.

TGA was performed to investigate the thermal properties of the prepared FGS/UPR nanocomposites. The results are demonstrated in Fig. 8 and Table 1. Compared with the neat UPR, the thermal decomposition temperatures at the maximum weight-loss rate (T_p) are improved for all the FGS/UPR nanocomposites, suggesting better thermal stability by the addition of GO inorganic additive. Furthermore, T_p increases with the increase of FGS content, and the maximum increase of 10.7 °C is achieved at a FGS content of 0.32 wt%. Specially, the functional groups on the dried nanosheets are decomposed at a no-so-high temperature (around 200 °C, as shown in Fig. S5†) and may serve as catalysts in deteriorating the thermal stability of the nanocomposites.[15,34] However, the FGS-based nanocomposites seems unaffected by this phenomenon, which is due to the interactions of FGS–polyesters and the partially thermal reduction of GO sheets during the *in situ* melt polycondensation process.[34,35]

DMA was conducted to study the thermo-mechanical properties of the FGS/UPR nanocomposites. The results are depicted in Fig. 9 and Table 1. The storage moduli at 40 °C of all the nanocomposites are higher than that of neat UPR, which suggest that the dynamic mechanical property of the UPR matrix is improved by the addition of GO additives. This result

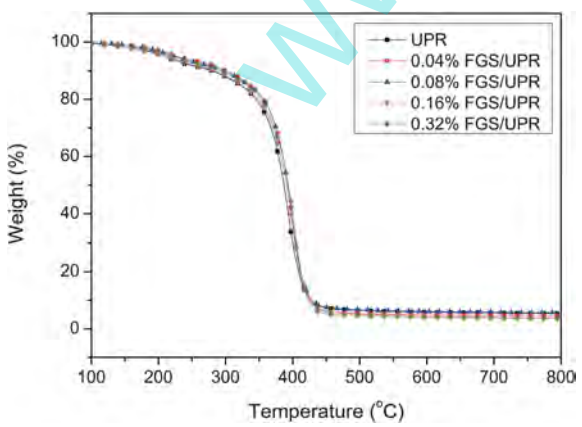

Fig. 8 TGA curves of neat UPR and FGS/UPR nanocomposites with different FGS contents.

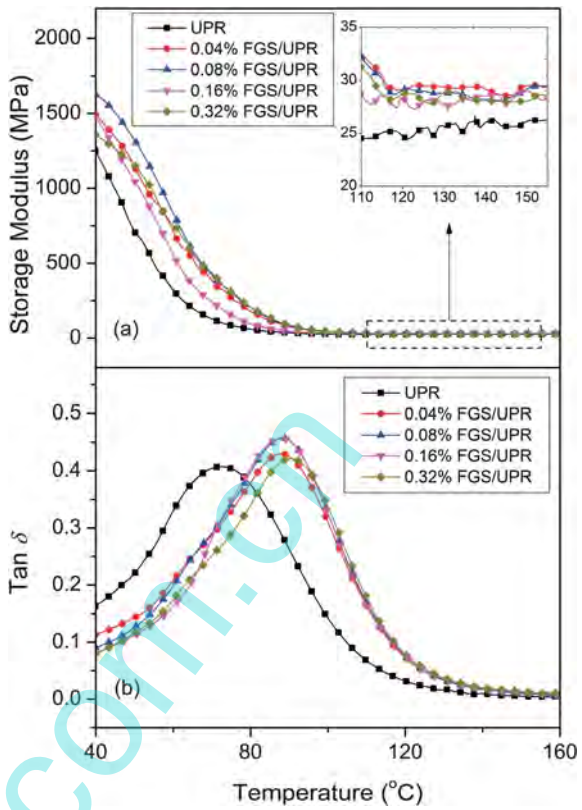

Fig. 9 DMA curves including (a) storage modulus and (b) loss factor of neat UPR and FGS/UPR nanocomposites with different FGS contents. The inset shows the magnified section of storage modulus at 110 to 155 °C.

is also demonstrated by the storage modulus in the rubbery region (150 °C in this study), as shown in the inset of Fig. 9a. These improvements also indicate the efficient load transfer from the matrix to the FGS nanofiller, which is caused by the good exfoliation of FGS and the strong FGS–polymer interaction. T_g is determined from the peaks of the loss factors (tan δ).[57] As shown in Fig. 9b and Table 1, T_g for the FGS/UPR composites improves by the addition of GO and increases with the increase of FGS content. With a FGS content of 0.32 wt% in the UPR matrix, T_g exhibits a maximum increase of 17.9 °C.

Conclusions

In this study, FGS/UPR nanocomposites have been successfully prepared by a convenient one-pot method integrating solvent-exchange method with *in situ* melt polycondensation. A novel solvent-exchange method involving fractional distillation has also been developed to prepare GO dispersions in EG solvent. The GO nanosheets have been exfoliated into individual nanosheets, and the concentrations of the as-prepared GO/EG dispersions is in the range of 1.47 to 13.0 mg ml^{-1}. A set of FGS/UPR nanocomposites with FGS contents of 0.04 to 0.32 wt% have been successively fabricated from the prepared GO/EG dispersions *via in situ* melt polycondensation. Structural characterization of these nanocomposites indicates that the FGS have been well exfoliated in the UPR matrix and strongly

interact with the UPR polymer. The stiffness, thermal stability, and thermo-mechanical properties of the nanocomposites are improved by the incorporation of GO nanosheets. Compared with the neat UPR matrix, the composite with low FGS content of 0.08 wt% exhibits maximum increases of 53.6% and 48.4% in tensile strength and modulus; the composite with 0.32 wt% FGS content shows 10.7 °C increase in T_p and 17.9 °C increase in T_g. Overall, the developed one-pot method does not alter the existing experimental apparatus for producing polyesters and simplifies the fabrication process of FGS/polyesters nanocomposites, thus holding great potential in industrial applications.

Acknowledgements

The authors are grateful to the National Natural Science Foundation of China (no. 31300489), the Chinese National Special Fund for International Cooperation of Science and Technology (no. 2011DFA32440), the Research Funds for Nanjing Institute of Technology (YKJ201002), and the Special Fund of Fundamental Research from Chinese Academy of Forest (no. CAFINT2011C02).

References

1 K. S. Novoselov, *Science*, 2004, **306**, 666–669.
2 S. Stankovich, D. A. Dikin, G. H. B. Dommett, K. M. Kohlhaas, E. J. Zimney, E. A. Stach, R. D. Piner, S. T. Nguyen and R. S. Ruoff, *Nature*, 2006, **442**, 282–286.
3 D. Chen, H. Feng and J. Li, *Chem. Rev.*, 2012, **112**, 6027–6053.
4 L. Chen, Y. Hernandez, X. Feng and K. Müllen, *Angew. Chem., Int. Ed.*, 2012, **51**, 7640–7654.
5 V. Georgakilas, M. Otyepka, A. B. Bourlinos, V. Chandra, N. Kim, K. C. Kemp, P. Hobza, R. Zboril and K. S. Kim, *Chem. Rev.*, 2012, **112**, 6156–6214.
6 D. Wu, F. Zhang, H. Liang and X. Feng, *Chem. Soc. Rev.*, 2012, **41**, 6160–6177.
7 L. Yan, Y. B. Zheng, F. Zhao, S. Li, X. Gao, B. Xu, P. S. Weiss and Y. Zhao, *Chem. Soc. Rev.*, 2012, **41**, 97–114.
8 X. Huang, X. Qi, F. Boey and H. Zhang, *Chem. Soc. Rev.*, 2012, **41**, 666–686.
9 D. R. Dreyer, S. Park, C. W. Bielawski and R. S. Ruoff, *Chem. Soc. Rev.*, 2010, **39**, 228–240.
10 M. Fang, K. G. Wang, H. B. Lu, Y. L. Yang and S. Nutt, *J. Mater. Chem.*, 2009, **19**, 7098–7105.
11 Y. K. Yang, C. E. He, R. G. Peng, A. Baji, X. S. Du, Y. L. Huang, X. L. Xie and Y. W. Mai, *J. Mater. Chem.*, 2012, **22**, 5666–5675.
12 H. X. Wei, Y. Y. Li, J. P. Chen, Y. Zeng, G. Q. Yang and Y. Li, *Chem.–Asian J.*, 2012, **7**, 2683–2689.
13 J. J. Liang, Y. Huang, L. Zhang, Y. Wang, Y. F. Ma, T. Y. Guo and Y. S. Chen, *Adv. Funct. Mater.*, 2009, **19**, 2297–2302.
14 Z. H. Tang, H. L. Kang, Z. L. Shen, B. C. Guo, L. Q. Zhang and D. M. Jia, *Macromolecules*, 2012, **45**, 3444–3451.
15 Y. Wang, Z. X. Shi, J. H. Fang, H. J. Xu and J. Yin, *Carbon*, 2011, **49**, 1199–1207.
16 J. Hong and J. Jang, *Soft Matter*, 2012, **8**, 7348–7350.
17 J. Li, F. Ye, S. Vaziri, M. Muhammed, M. C. Lemme and M. Östling, *Carbon*, 2012, **50**, 3113–3116.
18 X. Zhang, A. C. Coleman, N. Katsonis, W. R. Browne, B. J. van Wees and B. L. Feringa, *Chem. Commun.*, 2010, **46**, 7539–7541.
19 Y. T. Liang and M. C. Hersam, *J. Am. Chem. Soc.*, 2010, **132**, 17661–17663.
20 H. Hu, X. Wang, J. Wang, L. Wan, F. Liu, H. Zheng, R. Chen and C. Xu, *Chem. Phys. Lett.*, 2010, **484**, 247–253.
21 A. S. Patole, S. P. Patole, H. Kang, J.-B. Yoo, T.-H. Kim and J.-H. Ahn, *J. Colloid Interface Sci.*, 2010, **350**, 530–537.
22 J. R. Potts, S. H. Lee, T. M. Alam, J. An, M. D. Stoller, R. D. Piner and R. S. Ruoff, *Carbon*, 2011, **49**, 2615–2623.
23 M. A. Rafiee, J. Rafiee, I. Srivastava, Z. Wang, H. H. Song, Z. Z. Yu and N. Koratkar, *Small*, 2010, **6**, 179–183.
24 C. L. Bao, Y. Q. Guo, L. Song, Y. C. Kan, X. D. Qian and Y. Hu, *J. Mater. Chem.*, 2011, **21**, 13290–13298.
25 L. P. Yang, J. H. Kong, W. A. Yee, W. S. Liu, S. L. Phua, C. L. Toh, S. Huang and X. H. Lu, *Nanoscale*, 2012, **4**, 4968–4971.
26 F. Yavari, M. A. Rafiee, J. Rafiee, Z. Z. Yu and N. Koratkar, *ACS Appl. Mater. Interfaces*, 2010, **2**, 2738–2743.
27 A. K. Appel, R. Thomann and R. Mulhaupt, *Polymer*, 2012, **53**, 4931–4939.
28 X. Wang, Y. A. Hu, L. Song, H. Y. Yang, W. Y. Xing and H. D. Lu, *J. Mater. Chem.*, 2011, **21**, 4222–4227.
29 H. Kim, Y. Miura and C. W. Macosko, *Chem. Mater.*, 2010, **22**, 3441–3450.
30 Z. Xu and C. Gao, *Macromolecules*, 2010, **43**, 6716–6723.
31 S. Das, A. S. Wajid, J. L. Shelburne, Y. C. Liao and M. J. Green, *ACS Appl. Mater. Interfaces*, 2011, **3**, 1844–1851.
32 N. Du, C. Y. Zhao, Q. Chen, G. Wu and R. Lu, *Mater. Chem. Phys.*, 2010, **120**, 167–171.
33 Y. J. Huang, Y. W. Qin, Y. Zhou, H. Niu, Z. Z. Yu and J. Y. Dong, *Chem. Mater.*, 2010, **22**, 4096–4102.
34 D. Chen, H. Zhu and T. Liu, *ACS Appl. Mater. Interfaces*, 2010, **2**, 3702–3708.
35 K. Liu, L. Chen, Y. Chen, J. L. Wu, W. Y. Zhang, F. Chen and Q. Fu, *J. Mater. Chem.*, 2011, **21**, 8612–8617.
36 H. J. Salavagione, M. A. Gomez and G. Martinez, *Macromolecules*, 2009, **42**, 6331–6334.
37 H. L. Poh, F. Sanek, A. Ambrosi, G. J. Zhao, Z. Sofer and M. Pumera, *Nanoscale*, 2012, **4**, 3515–3522.
38 T. Hartono, S. B. Wang, Q. Ma and Z. H. Zhu, *J. Colloid Interface Sci.*, 2009, **333**, 114–119.
39 W. S. Hummers and R. E. Offeman, *J. Am. Chem. Soc.*, 1958, **80**, 1339.
40 N. I. Kovtyukhova, P. J. Ollivier, B. R. Martin, T. E. Mallouk, S. A. Chizhik, E. V. Buzaneva and A. D. Gorchinskiy, *Chem. Mater.*, 1999, **11**, 771–778.
41 J. I. Paredes, S. Villar-Rodil, A. Martínez-Alonso and J. M. D. Tascón, *Langmuir*, 2008, **24**, 10560–10564.
42 G. X. Wang, B. Wang, J. Park, J. Yang, X. P. Shen and J. Yao, *Carbon*, 2009, **47**, 68–72.
43 L. Lai, L. Chen, D. Zhan, L. Sun, J. Liu, S. H. Lim, C. K. Poh, Z. Shen and J. Lin, *Carbon*, 2011, **49**, 3250–3257.

44 C. L. Bao, L. Song, C. A. Wilkie, B. H. Yuan, Y. Q. Guo, Y. Hu and X. L. Gong, *J. Mater. Chem.*, 2012, **22**, 16399–16406.
45 T. Nakajima, A. Mabuchi and R. Hagiwara, *Carbon*, 1988, **26**, 357–361.
46 M. Skrifvars, P. Niemel, R. Koskinen and O. Hormi, *J. Appl. Polym. Sci.*, 2004, **93**, 1285–1292.
47 C. M. S. Izumi and M. L. A. Temperini, *Vib. Spectrosc.*, 2010, **54**, 127–132.
48 J. Maultzsch, S. Reich and C. Thomsen, *Phys. Rev. B: Condens. Matter Mater. Phys.*, 2004, **70**, 155403.
49 K. N. Kudin, B. Ozbas, H. C. Schniepp, R. K. Prud'homme, I. A. Aksay and R. Car, *Nano Lett.*, 2008, **8**, 36–41.
50 M. C. Hsiao, S. H. Liao, M. Y. Yen, P. I. Liu, N. W. Pu, C. A. Wang, N. W. Pu, H. M. Tsai and C. C. M. Ma, *ACS Appl. Mater. Interfaces*, 2010, **2**, 3092–3099.
51 H. X. Wang, K. G. Zhou, Y. L. Xie, J. Zeng, N. N. Chai, J. Li and H. L. Zhang, *Chem. Commun.*, 2011, **47**, 5747–5749.
52 B. W. Zhang, Y. J. Zhang, C. Peng, M. Yu, L. F. Li, B. Deng, P. F. Hu, C. H. Fan, J. Y. Li and Q. Huang, *Nanoscale*, 2012, **4**, 1742–1748.
53 T. Ramanathan, A. A. Abdala, S. Stankovich, D. A. Dikin, M. Herrera-Alonso, R. D. Piner, D. H. Adamson, H. C. Schniepp, X. Chen, R. S. Ruoff, S. T. Nguyen, I. A. Aksay, R. K. Prud'homme and L. C. Brinson, *Nat. Nanotechnol.*, 2008, **3**, 327–331.
54 H. Kim, A. A. Abdala and C. W. Macosko, *Macromolecules*, 2010, **43**, 6515–6530.
55 D. R. Dreyer, K. A. Jarvis, P. J. Ferreira and C. W. Bielawski, *Polym. Chem.*, 2012, **3**, 757–766.
56 X. S. Du, Z. Z. Yu, A. Dasari, J. Ma, M. S. Mo, Y. Z. Meng and Y. W. Mai, *Chem. Mater.*, 2008, **20**, 2066–2068.
57 C. G. Liu, Y. Dai, C. S. Wang, H. F. Xie, Y. H. Zhou, X. Y. Lin and L. Y. Zhang, *Ind. Crops Prod.*, 2013, **43**, 677–683.